REVISTA MATÉRIA V.27 N.02
ISSN 1517-7076 articles e13172, 2022

The effect of cationic, anionic and nonionic surfactants on morphology and antibacterial properties of zinc oxide

Mobina Bazari[1], Najmeh Najmoddin[1]

[1]Department of Biomedical Engineering, Science and Research Branch, Islamic Azad University, Shohada Hesarak Blvd, Daneshgah Square, Sattari Highway, PO Box 14975/112, Postal code 1497713115, Tehran, Iran.
email: mb.bazari@yahoo.com; najmoddin@srbiau.ac.ir (correspondence)

ABSTRACT

In this study, zinc oxide was synthesized through wet chemical method at room temperature (RT), 40 °C and 60 °C without surfactant and at the presence of cetyltrimethylammonium bromide (CTAB), sodium dodecyl sulfate (SDS) and polyethylene glycol (PEG 6000) as cationic, anionic and non-ionic surfactants, respectively. Field emission scanning electron microscopy (FESEM) was used to investigate the effect of temperature and type of surfactants on the morphology of zinc oxide. FESEM images showed that the morphology of zinc oxide changed from rod-like at room temperature with increasing temperature. The morphology of zinc oxide samples synthesized by CTAB, SDS, and PEG surfactants was worm-like, nut-like and rod-like, respectively. The results of X-ray diffraction spectroscopy (XRD) analysis indicated the presence of zinc oxide phase in all samples. $Zn(OH)_2$ phase was also detected in the sample synthesized with PEG 6000. Fourier-transform infrared spectroscopy (FTIR) analysis was used to evaluate the functional groups. Antibacterial activity of zinc oxide samples against *Staphylococcus aureus* (*S. aureus*) and *Escherichia coli* (*E. coli*) strains was evaluated by using disc diffusion technique and colony-forming unit (CFU) method. Both methods confirmed the antibacterial activity of all samples. Moreover, the highest antibacterial activity was shown for the sample synthesized in the presence of PEG as a surfactant.

Keywords: Zinc oxide; Surfactant; Antibacterial activity; Morphology

1. INTRODUCTION

Zinc oxide (ZnO) has received more attention in various applications such as varistors [1], solar cells [2], gas sensors [3], sun creams [4], skin cosmetics along with medical applications [5] like burn treatment and skin diseases such as eczema due to their unique properties including wide energy band gap [6], excellent chemical and thermal stability [7], specific electrical and optoelectronic properties [8], excellent antibacterial effect [9, 10], UV light adsorbent [11], as well as non-toxicity [12].

Various methods including thermal decomposition [13], hydrothermal method [14], solution-combustion method [15], sol-gel [16], spray pyrolysis [17], sonochemical synthesis [18], microwave-assisted synthesis [19], wet chemical [20], etc. have been used to produce different morphologies of ZnO such as wire, tube, rod, ribbons and spheres [21]. Chemical synthesis methods such as wet chemical, precipitation, sol-gel, etc., are among the popular methods due to their ability to control morphology, purity, crystallinity, composition and particle growth at relatively low temperature as well as their simplicity and inexpensiveness [22].

Surfactants play an important role in the morphology and particle size of ZnO. IQBAL, *et al.* [23] reported the synthesis of needle-like and plate-like ZnO nanoparticles using cetyltrimethylammonium bromide (CTAB) as a cationic surfactant and sodium dodecyl sulfate (SDS) as an anionic surfactant. DEBANATH and KARMAKAR [24] reported the synthesis of zinc oxide nanoparticles using polyvinylpyrrolidone (PVP). ZARE, *et al.* [25] synthesized flower-like nanoflakes zinc oxide using oleic acid ($C_{18}H_{34}O_2$) surfactant.

Aqueous ZnO suspension enhances reactive oxygen species (ROS), hydroxyl radicals ($^{\bullet}OH$), hydrogen peroxide (H_2O_2), and peroxide (O_2^{-2}), which contribute to the antibacterial activity of ZnO [26]. In this regard, SIRELKHATIM, *et al.* [26] presented a theory on the antibacterial properties of ZnO nanostructures. Antibacterial behavior of ZnO nanostructures against *E. coli* and *S. aureus* with rod, sphere and flower shape obtained through different solvents was investigated by TALEBIAN, *et al.* [27]. CHITRA and ANNADURAI [28] reported the antibacterial activity of spherical ZnO nanoparticles against two bacteria, *E. coli* and *Pseudomonas aeruginosa*. Growth inhibition of *C. albicans* bacteria by flower-like and mulberry-like

Corresponding Author: Najmeh Najmoddin
Received on: 18/10/2020 Accepted on: 31/01/2022

10.1590/S1517-707620220002.1372

ZnO structures was reported by MA, *et al.* [29]. RAMANI, *et al.* [30] reported the antibacterial effect of plate-like and rod-like ZnO against *S. aureus*, S. *typhimurium*, *P. vulgaris* and *K. pneumoniae*. On the other hand, using various types of surfactants can also affect the antibacterial properties of ZnO. The antibacterial effect of ZnO nano-drums synthesized with fructose as a nonionic surfactant was investigated by IQBAL, *et al.* [23]. Similarly, ZARE, *et al.* [25] investigated the antibacterial properties of flower-like nanoflakes ZnO synthesized with oleic acid ($C_{18}H_{34}O_2$) surfactant. Moreover, the antibacterial properties of nanoflake and nanoflower zinc oxide synthesized with cationic surfactant HY (alkyl (hydroxy-ethyl) dimethyl ammonium chloride) as well as zinc oxide nanosheets synthesized with anionic surfactant SDS were studied by EL-NAHHAL *et al.* [31].

As mentioned before, there are many reports regarding the synthesis of ZnO structures with different methods. Many of these methods have been used toxic and expensive materials, long reaction time, and high temperature. However, there are rare reports on the synthesis of ZnO structures through simple wet chemical method using cationic, anionic, and nonionic surfactants with their effects on the antibacterial activity of ZnO. In this study, ZnO was synthesized by wet chemical method at room temperature (RT), 40 °C and 60 °C and using different surfactants (CTAB, SDS, polyethylene glycol (PEG)). Systematic studies have been done to investigate the effect of different surfactants on the morphology and antibacterial properties of ZnO structures.

2. MATERIALS AND METHODS

2.1 Synthesis of ZnO

Zinc nitrate ($Zn(NO_3)_2.6H_2O$, ≥99.5%, Sigma Aldrich), sodium hydroxide (NaOH, ≥99%, Merck), ammonia (NH_3, Merck), ethylene diamine (EDA, ≥98%, Merck), cetyltrimethylammonium bromide (CTAB, Merck), sodium dodecyl sulfate (SDS, Merck), polyethylene glycol (PEG 6000, Merck), pure ethanol (≥99.99%, Merck) and deionized water were used in this experiment. All the reagents used were of analytical grade without further purification.

Certain amount of $Zn(NO_3)_2.6H_2O$ and NaOH were dissolved in deionized water, separately. The $Zn(NO_3)_2.6H_2O$ solution was then added drop-wise to the aqueous solution of NaOH under the stirring to obtain a clear solution. The resulting solution was transferred to a 250 mL plastic beaker and then certain amount of pure ethanol and EDA were added to the above solution, respectively. The room temperature (RT) was monitored using a thermometer and the average temperature was 30 °C. The final mixture was kept at RT, 40 °C and 60 °C respectively for 24 h. After the reaction, the precipitate was filtered and washed several times with deionized water and alcohol and then dried at 60 °C in air overnight.

Table 1: Process variables and synthesized samples

Sample / Parameters	SAMPLES WITHOUT SURFACTANT (WS)	CTAB-RT	SDS-110	PEG-70
Final temperature	RT, 40 °C, 60 °C	RT	110 °C	70 °C
Zinc nitrate	1.478 g	2.974 g	5.229 g	1.405 g
Sodium hydroxide	6 g	8 g	3.839 g	-
Ammonia	-	-	-	25 cc
Pure ethanol	100 cc	100 cc	-	-
Deionized water	10 cc	20 cc	78 cc	250 cc
EDA	30 cc	10 cc	-	-
CTAB	-	0.4 g	-	-
SDS	-	-	0.288 g	-
PEG	-	-	-	0.5 g

Products were signed as WS-RT, WS-40 and WS-60, respectively. CTAB, SDS and PEG were used to investigate the role of cationic, anion and nonionic surfactants on the morphology and antibacterial activity of ZnO. Similar procedure was adopted for samples containing surfactants with minor changes. For synthesis of sample containing CTAB (CTAB-RT), a certain amount of CTAB was added to the NaOH solution. For the sample containing SDS surfactant (SDS-110), a certain amount of SDS was dissolved in deionized water

and then the SDS solution was added to the mixture of $Zn(NO_3)_2.6H_2O$ and NaOH. In the case of the sample containing PEG (PEG-70), instead of using NaOH solution, a solution of PEG and ammonia was added to the $Zn(NO_3)_2.6H_2O$ solution. The detailed information about the synthesis condition of ZnO is given in Table 1. Schematic of the preparation of the ZnO samples are shown in Figure 1.

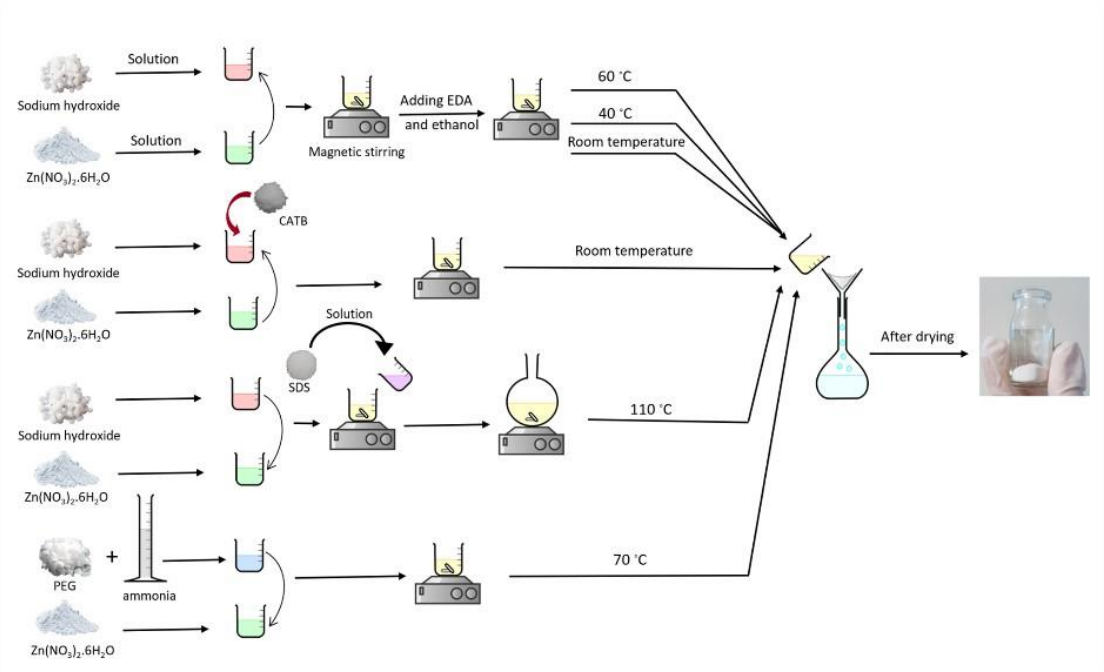

Figure 1: Schematic of the preparation of the ZnO samples.

2.2 Characterization

Crystal structure of the samples was performed by X-ray diffraction spectroscopy (XRD) model ETOE made in Germany using a CuKα lamp with 40 kV voltage and 40 mA current over the range of 2θ = 20°-80°. The morphology of the samples was investigated by field emission scanning electron microscope (FE-SEM) HITACHI S-4160 model made in Japan. For the FE-SEM analysis, the ZnO samples were dispersed in pure ethanol in an ultrasonic aqueous bath before testing. Fourier-transform infrared spectroscopy (FTIR) analysis was performed to investigate the functional groups existed at the ZnO surface.

2.3 Antibacterial assay

Antibacterial activity of ZnO samples against strains of *S. aureus* (gram positive) and *E. coli* (gram negative) was evaluated by disc diffusion and colony-forming unit (CFU) methods. All materials were sterilized in an autoclave before testing. The nutrient broth (NB) and nutrient agar medias were used to culture the *S. aureus* and *E. coli* bacterias at 37 °C with shaking (200 rpm) in the incubator. In the disc diffusion method (antibiogram disc diffusion), 10 mg of each ZnO sample were incubated at 37 °C for 24 h after being placed in the culture medium. It should be noted that Gentamicin discs (10 µg antibiotics) were used as a control sample. After 24 h, the antibacterial activity of the samples was evaluated by the measuring the diameter of the inhibitation zone formed around the specimens. In CFU method, for microbial suspension preparation, 100 µl of suspension of each bacteria with a concentration of 107 CFU/ml was put adjacent to the liquid growth medium (Nutrient Broth) and after vortex, was incubated at 37 °C with shaking (200 rpm) for 24 h. Then, 1 ml of the growth medium containing the bacteria cultured adjacent to the specimen, was removed and diluted using 9 ml double distilled water at OD_{600} = 0.8 (optical density), which is the suitable optical density of cells and then ZnO samples were added into the solution. Solution dilution was performed once more with a 1 to 10 ratio. Finally, 10 µl of the said solution was cultured in a solid nutrient agar medium and then incubated for 24 h to grow bacterial colonies. After 24 h, the number of bacterial colonies was counted by a colonometer. ZnO-free culture medium, under the same reaction conditions, was used as control sample after culture [26].

3. RESULTS AND DISCUSSION

3.1 Morphology analysis

3.1.1 Surfactant-free samples

The morphology of the ZnO samples without surfactants at RT, 40 °C and 60 °C are shown in Figure 2. FESEM images showed the WS-RT sample had rod-like morphology. As the temperature increased, it was observed that the ZnO morphology deviated from the rod-like to irregular and agglomerated state.

The mechanism of ZnO formation is through the following route:

$$Zn^{2+} + 4OH^{-} \rightarrow Zn(OH)_4^{2-} \quad (1)$$

$$Zn(OH)_4^{2-} \rightarrow ZnO + H_2O + 2OH^{-} \quad (2)$$

It has been reported that the molar ratio of Zn^{2+}/OH^{-} during synthesis should be at least 1:4 for the reaction to proceed [32]. For Zn^{2+}/OH^{-} higher than 1:40, no precipitate is formed due to the high amount of OH^{-} in the solution [32, 33]. Since the molar ratio of Zn^{2+}/OH^{-} in this synthesis was 1:30, ethanol was used to deactivate the OH^{-} ions. Therefore, the reaction (2) moved to the right (ZnO formation). In alkaline synthesis, the zinc anionic species $Zn(OH)_4^{2-}$ is strongly adsorbed on the (0001) face of the ZnO crystal, which in this case, growth along the (002) direction (c axis) increases, which leads to better growth and increase the aspect ratio of ZnO [27]. On the other hand, EDA was added as an adsorbing ligand [34] that binds to Zn^{2+} cations, thereby reducing the radial growth of the rods. It has been revealed that increasing temperature over 60 °C may accelerate agglomeration phenomenon and facilitate the particle growth which consequently influences the ZnO morphology and particle size [35-37]. Moreover, the lowest temperature for formation of ZnO powder has been reported to be 25 °C [36, 37].

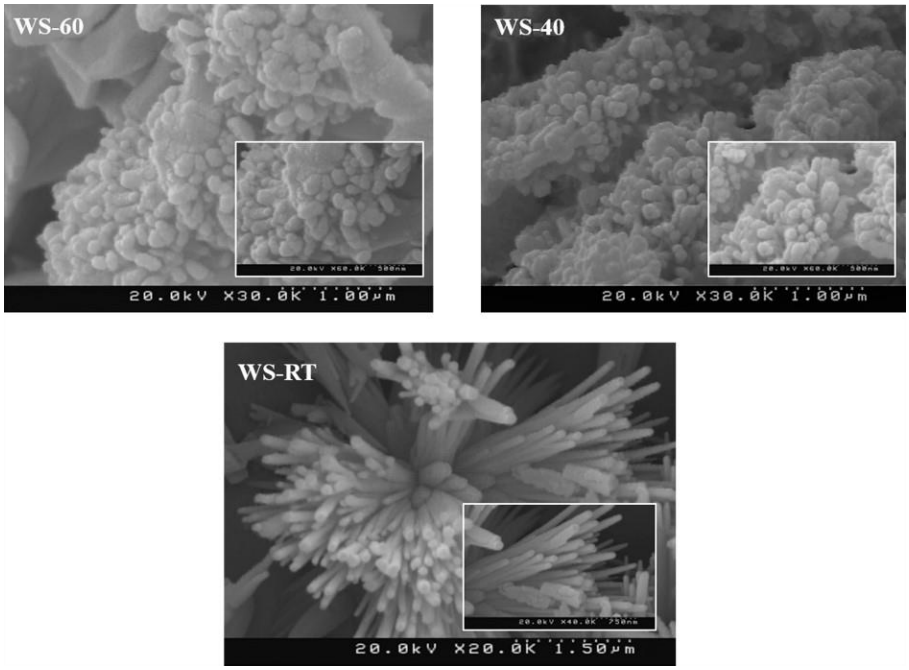

Figure 2: FESEM images of synthesized ZnO samples at different reaction temperatures: room temperature, 40 °C and 60 °C. Images of the WS-40 and WS-60 samples were taken at ×30K and ×60K magnification and the WS-RT sample at ×20K and ×40K magnification, respectively.

3.1.2 Surfactant-containing samples

In order to investigate the role of surfactant on the growth of ZnO structures, CTAB-RT, SDS-110 and PEG-70 were synthesized in the presence of cationic, anionic and nonionic surfactants. The FESEM images (Figure 3) showed that the morphology of the samples changed significantly with the type of the surfactants.

Moreover, all samples showed distinct, homogeneous and non-agglomerated structures.

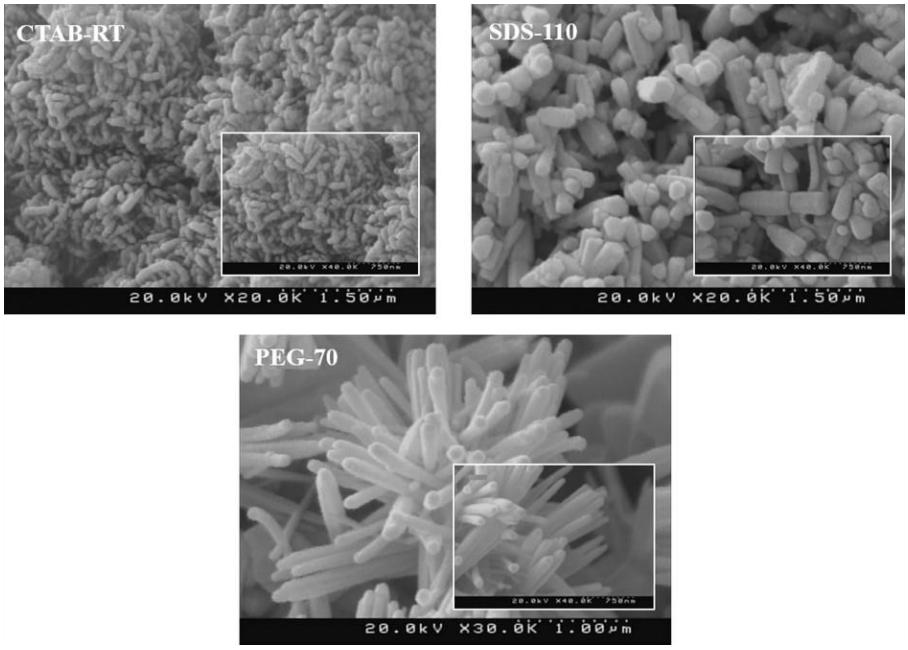

Figure 3: FESEM images of synthesized ZnO samples in the presence of CTAB, SDS and PEG surfactants. Images of the SDS-110 and CTAB-RT samples were taken at magnification of ×20K and ×40K and images of sample PEG-70 at ×30K and ×40K, respectively.

As can be seen, the CTAB-RT sample had worm-like morphology. Due to the presence of surfactant, the surface tension of the solution decreases thereby reduces the energy needed to form a new phase [38]. Therefore, ZnO crystals can form at lower saturation [38]. In addition, one of the important factors affecting the growth rate and crystal orientation is how the units of growth are adsorbed on the crystal surfaces [38], which is a function of the type of surfactant interaction with the growth unit. In the ZnO growth process, CTAB surfactant absorbed to the negative charge $Zn(OH)_4^{2-}$, due to its positive charge and could be considered as a carrier for $Zn(OH)_4^{2-}$. As shown in Figure 4, these ion pair form a film on the surface of the ZnO crystal and the growth process continue by releasing the growth units onto the crystal surface. Also, in the crystallization process, the surfactant molecules prevented the agglomeration by controlling the growth process by forming this film on the ZnO crystal. CTAB can also accelerate the reaction rate [38]. RANA, *et al.* [39] reported spherical morphology for ZnO synthesized in the presence of CTAB. The discrepancy between their results and ours could be related to the reaction temperature and the step of adding CTAB surfactant during synthesis.

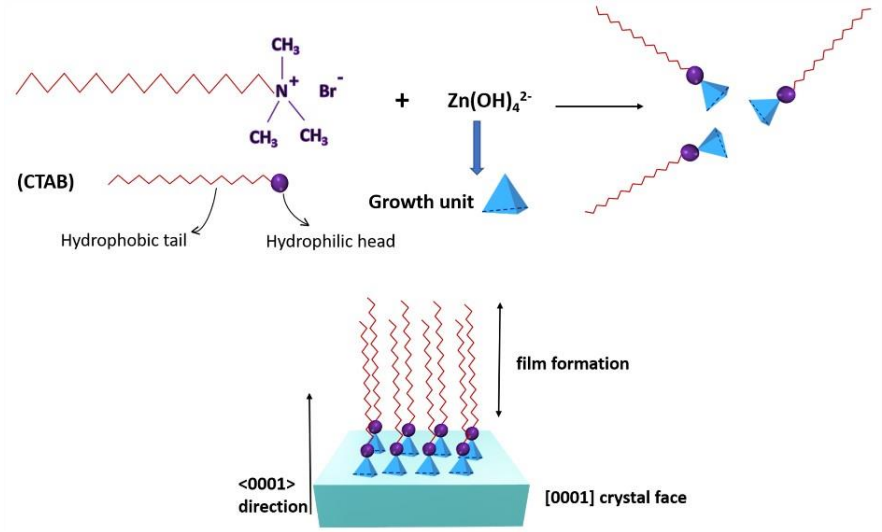

Figure 4: The mechanism of ZnO formation in the presence of CTAB surfactant.

In the SDS-110 sample, the addition of anionic surfactant resulted in ZnO structures with nut-like morphology. This could be attributed to the type of interaction between SDS surfactant and the surfaces of ZnO crystals. SDS is known as a gemini surfactant, which can be described as two independent surfactant molecules connected by a bridge [40]. The SDS molecule contains SO_4^{2-} which is absorbed by (0001) face of ZnO crystal due to the presence of positive charge Zn^{2+} ions on this face. As shown in Figure 5, in fact, each germinal SDS can simultaneously absorb two ZnO nuclei on the (0001) face due to the Columbus force function. Therefore, SDS can adhere two (0001) faces. As a result, growth is restricted to the c-axis direction and can only occur in the (0001) face, with the lowest growth rate. As a result, twin nut-like structure of ZnO was formed. WANG, *et al.* [41] synthesized ZnO nanorods in the presence of SDS, which differs with the morphology of the SDS-110 in this study. The reason for this difference may be due to the use of $Zn(OH)_2$ as the main reactant instead of zinc nitrate in their work.

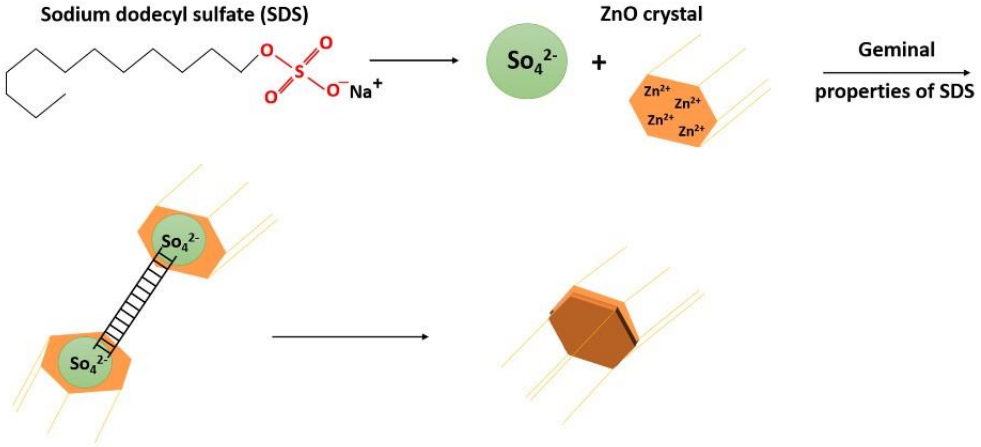

Figure 5: Formation of nut-like ZnO in the presence of SDS.

In the sample containing PEG (PEG-70), in addition to $Zn(OH)_4^{2-}$, $Zn(NH_3)_4^{2+}$ could also be formed as a growth unit according to the following reactions:

$$Zn^{2+} + 4NH_3 \rightarrow Zn(NH_3)_4^{2+} \tag{3}$$

$$Zn(NH_3)_4^{2+} + 2OH^- \rightarrow ZnO + 4NH_3 + H_2O \tag{4}$$

By adding PEG, these growth units are easily absorbed by the O atom in the C-O-C chain. In fact, PEG can act as a carrier for these ions and transport them to the site of crystalline ZnO particles. Therefore, growth occurs at active sites around the surface of the ZnO core [42]. In this case, the growth of ZnO crystals occurs in the [0001] direction. Temperature increment to 70°C, increases the rate of production of $Zn(NH_3)_4^{2+}$ growth units in the reaction system. When the growth rate corresponds to the rate of formation of the ZnO core, only rod structures are formed at 70 °C. The mechanism of the efficacy of this surfactant is shown in Figure 6. Therefore, PEG-70 had rod-like morphology with higher dispersion and quality than the WS-RT sample. SUDHA, *et al.* [43] reported nanospheres ZnO in the presence of PEG, which differs from the morphology of PEG-70 in this paper. The reason can be attributed to the use of ammonia instead of sodium hydroxide in our research and also the synthesis temperature.

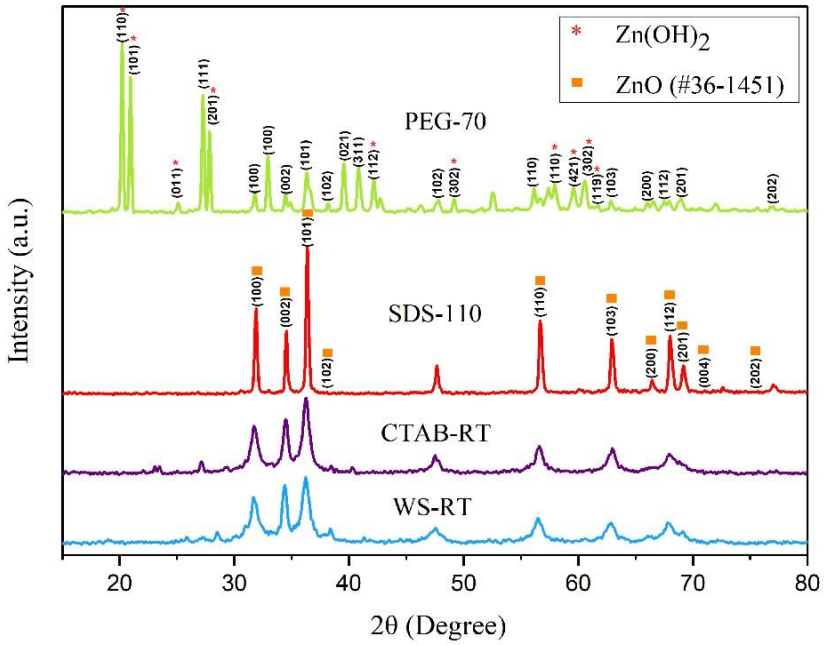

Figure 6: Formation of ZnO rods in the presence of PEG.

3.2 Structural analysis

The XRD spectra of ZnO structures are shown in Figure 7. In all samples, sequences of structural peaks: 31.77° (100), 34.42° (002), 36.25° (101), 47.53° (102), 56.60° (110), 62.86° (103), 66.38° (200), 67.96° (112) and 69.10° (201) were seen, which were in agreement with the ZnO structure (JCPDS#36-1451) [32]. In the PEG-70 sample, in addition to the above peaks, the structural peaks 20.21° (110), 20.91° (101), 25.10° (011), 27.84° (201), 42.17° (112), 47.83° (302), 57.40° (110), 59.59° (421), 60.66° (302) and 62.85° (119) were observed respectively, which were consistent with the structure of $Zn(OH)_2$ (JCPDS#48-1066). All three CTAB-RT, SDS-110, and WS-RT samples exhibited the same diffraction pattern without any impurity, suggesting the formation of ZnO with hexagonal phase. SDS-110 sample spectrum had a higher peak intensity than the other two samples. EADI *et al*. reported that SDS has a positive effect on the crystallinity of ZnO powders. In this procedure, (SO_4^{2-}) unit was absorbed to the (0001) face of ZnO from a nut-like structure and the (SO_4^{2-}) unit was sandwiched between two (0001) faces and ZnO crystal growth happened along (0001) faces [44]. The difference between the pattern of PEG-70 and other samples could be due to the presence of the $Zn(OH)_2$ along with ZnO [41].

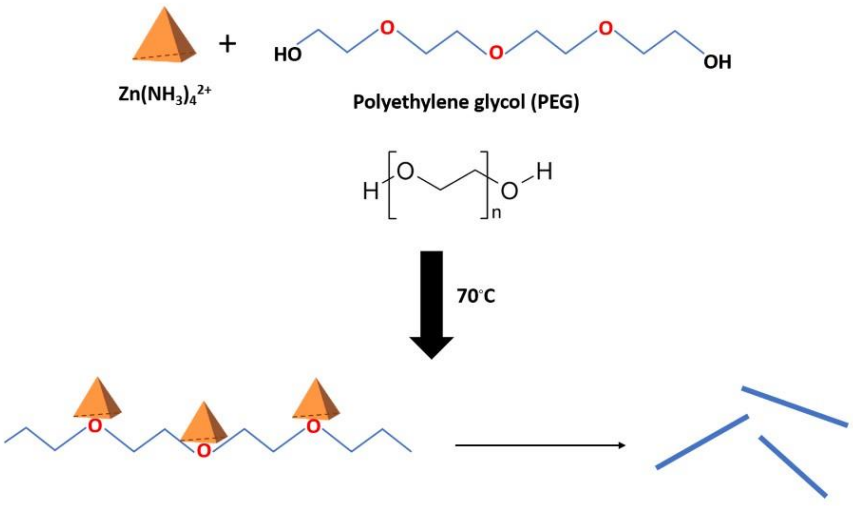

Figure 7: Powder X-ray diffraction pattern of synthesized ZnO samples.

3.3 Fourier-transform infrared spectroscopy analysis (FTIR)

The functional groups of the samples were analyzed by FTIR spectroscopy. The FTIR spectra of WS-RT, CTAB-RT, SDS-110 and PEG-70 in the range of 600-4000 cm^{-1} are shown in Figure 8. The major peaks of WS-RT samples were observed at (3669 and 3421), (2976 and 2920), 1388, 1250 and 890 cm^{-1}, which were related to O-H stretching, C-H stretching, C-H bending, C-O stretching and formation of tetrahedral coordination of Zn, respectively [45].

The CTAB-RT sample spectra showed characteristic peaks (3646 and 3391), (2922 and 2908), 1377, 1176, and 867 cm^{-1}, which were related to O-H stretching, C-H stretching, C-H bending, C-N stretching, and formation of tetrahedral coordination of Zn, respectively. Higher intensity and peak broadening were seen at 3391 cm^{-1} and 1377 cm^{-1} in the CTAB-RT sample compared to the WS-RT sample [23, 39].

The characteristic peaks of SDS-110 were observed at (3746 and 3437), (2924 and 2904), 1384, (1256 and 1102), 879 and 650 cm^{-1} which were related to O-H stretching, C-H stretching, S=O stretching, C-O stretching, formation of tetrahedral coordination of Zn and stretching vibration of ZnO band, respectively. The band intensities also decreased in SDS-110 sample compared to WS-RT sample [23, 41].

In the PEG-70 spectra, the characteristic peaks appeared at (3744 and 3232), 1461, 1251, (1091 and 1030), and (849 and 773) cm^{-1} were related to O-H stretching, C-H bending, C-O stretching, C-O stretching and formation of tetrahedral coordination of Zn, respectively. Higher peak broadening related to O-H stretching vibration of PEG-70 compared to the WS-RT sample could be due to the presence of OH group in the structure of PEG along with OH group in $Zn(OH)_2$ detected in the XRD pattern of this sample [46].

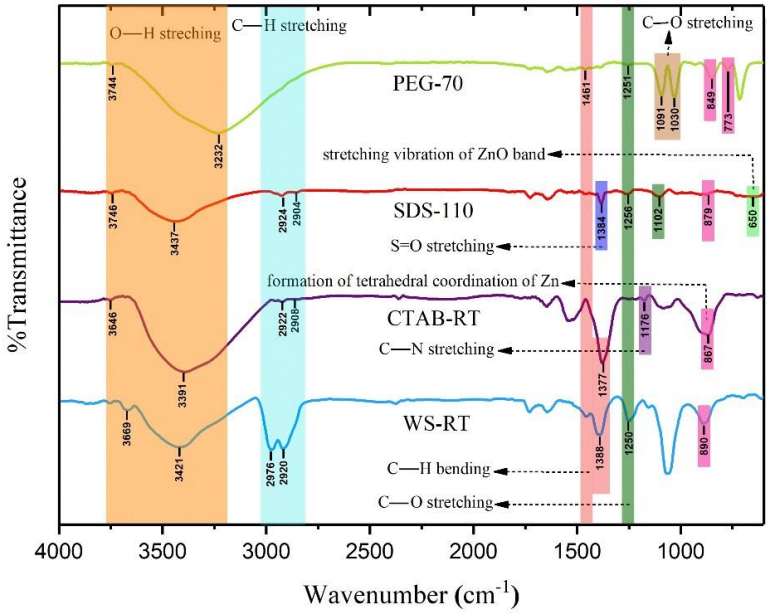

Figure 8: FTIR spectra of ZnO structures.

3.4 Antibacterial analysis

The antibacterial ability of ZnO structures was examined by disc diffusion method, which involves the destruction of the bacterial wall. Antibacterial agents are drugs with selective concentrations that are capable of damaging or inhibiting bacterial growth and are not harmful to the host [47]. These compounds act as chemicals to treat or prevent bacterial infections [23, 47]. The inhibition zone is an area where bacterial growth is stopped due to the antibacterial property of the sample [23]. The diameter of the inhibitory zone indicates the antibacterial activity of the sample [23]. Antibacterial activity of ZnO structures is attributed to various mechanisms including direct contact of ZnO structures with bacterial cell wall, integrated destruction of bacterial cells, release of antibacterial ions such as Zn^{2+} from ZnO, and formation of reactive oxygen species (ROS) which can damage the bacterial cell wall [26]. ROS include superoxide anion ($O_2^{\bullet-}$), hydrogen peroxide (H_2O_2), and hydroxide (OH^-). The toxicity of these species involves the destruction of cellular components such as lipids, DNA, and proteins. Another mechanism involved in the elimination of bacteria is the release of Zn^{2+} from the ZnO sample. The released Zn^{2+} has an important role in inhibiting active transport, as well as amino acid metabolism and disruption of the enzyme system.

Figure 9 shows the extent of growth inhibition by WS-RT, CTAB-RT, SDS-110 and PEG-70 samples against *E. coli* and *S. aureus* strains. All ZnO samples showed stronger antibacterial activity against *S. aureus* (gram positive) strain than *E. coli* (gram negative) strain. The reason for this is attributed to the different cell wall structure of these two species of bacteria. The cell wall of gram-positive strain is relatively simple and has a cytoplasmic membrane with multi-layered polymeric peptidoglycans and a thick cell wall (20 to 80 nm) [48]. Whereas, the gram-negative cell wall is composed of two cell membranes, one outer membrane and one plasma membrane with a thin layer of peptidoglycan with thickness of 7-8 nm. Therefore, compared to gram-positive bacteria, gram-negative strains are more resistant to antibiotics because of their impenetrable wall. Among the synthesized zinc oxide samples, the PEG-70 showed the highest antibacterial activity in disc diffusion test.

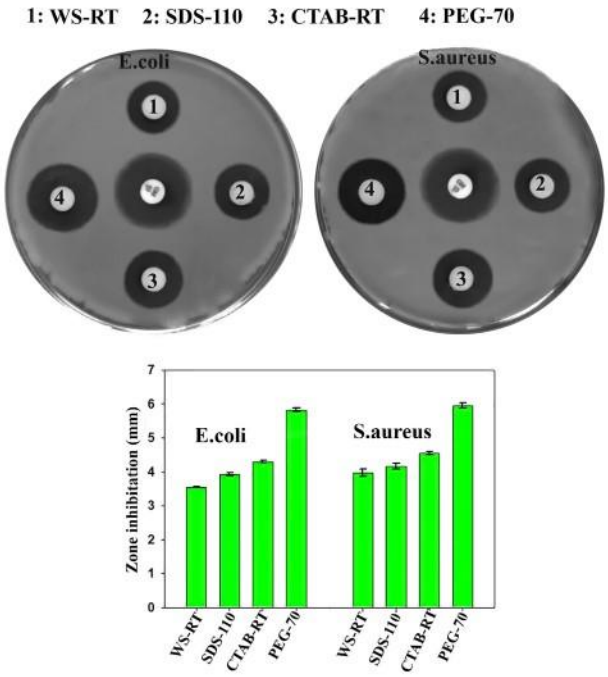

Figure 9: Inhibition zone for WS-RT, CTAB-RT, SDS-110 and PEG-70 samples against *E. coli* and *S. aureus.*

Figure 10 and Table 2 show the number of colonies formed by both *E. coli* and *S. aureus* strains for WS-RT, CTAB-RT, SDS-110 and PEG-70 samples. Similar to the disc diffusion test, the activity of both bacterial strains was restricted by all samples, and the number of colonies per sample was lower for *S. aureus* than for *E. coli*. According to the growth inhibition test (the disc diffusion test) and the CFU method, the antibacterial activity of the ZnO samples, from lowest to highest, was WS-RT < SDS-110 < CTAB-RT < PEG-70, respectively. Factors affecting the antibacterial properties of ZnO include morphology, particle size and concentration, surface properties, etc. The results showed that the antibacterial effect of the CTAB-RT was greater than SDS-110, which may be related to the amount of ROS formation by the sample. According to FTIR analysis, the CTAB-RT sample had a stronger O-H bond than the SDS-110 sample, which could exacerbate ROS and antibacterial activity [26].

Table 2: Report on the number of colonies formed of all synthesized zinc oxide samples against *S. aureus* and *E. Coli* bacteria.

Sample	E. coli	S. aureus
Control	869±78	764±45
WS-RT	245±12	128±23
SDS-110	210±11	98±25
CTAB-RT	14±3	9±1
PEG-70	7±1	4±2

According to data obtained from disc diffusion test and CFU method, the highest antibacterial activity was related to the sample of PEG-70. According to XRD *analysis*, this sample contained $Zn(OH)_2$ phase. According to FTIR analysis, due to the presence of $Zn(OH)_2$ as well as the presence of O-H bond in PEG structure, stronger O-H bond was observed in this sample which could increase generation of ROS and in this way, it improves antibacterial activity [26]. Moreover, it has been reported that the rod and wire shape of ZnO penetrate into cell walls of bacteria more easily than spherical one [26]. Therefore, it is expected that rod-like morphology of PEG-70 also contributes to the antibacterial activity of this sample. The antibacterial effect of the ZnO sample in the presence of PEG was also reported by NAIR, *et al.* [49] using CFU assay. In NAIR, e*t al.* study, loss of *E. coli* membrane before and after ZnO exposure, was investigated by SEM. Thus, the simultaneous antibacterial effect of PEG and $Zn(OH)_2$ duo to the presence of OH group as well as rod-like morphology of PEG-70, caused the highest antibacterial property of this sample among the other ones in this study.

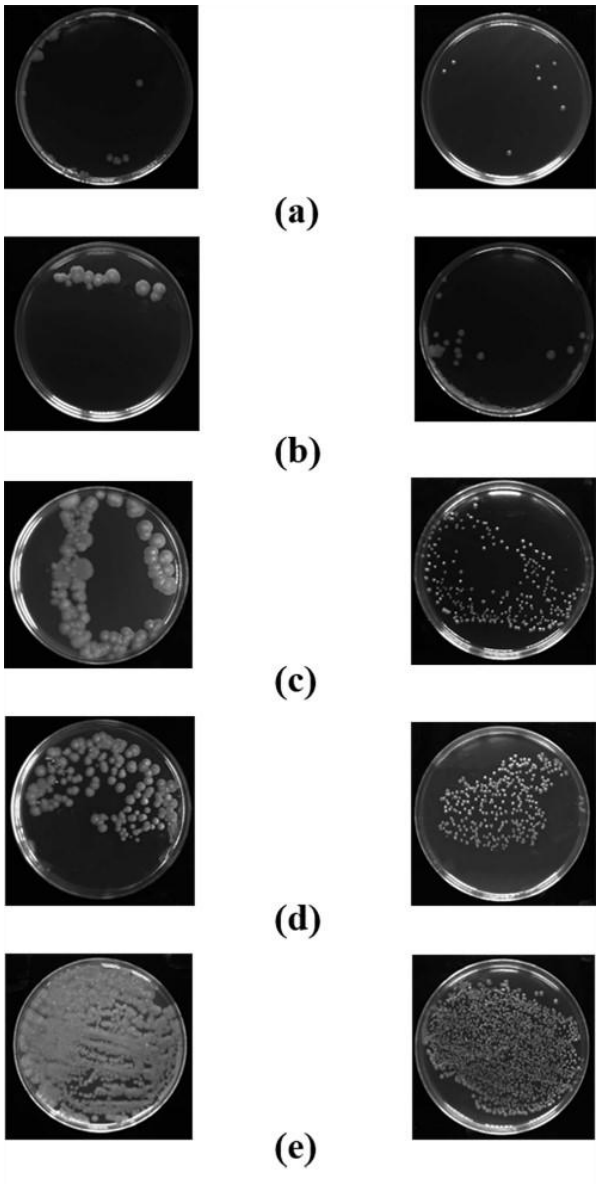

Figure 10: Colonies formed against *S. aureus* (**left**) and *E. coli* (**right**) for samples (a) PEG-70 (b) CTAB-RT (c) SDS-110 (d) WS-RT (e) Control.

4. CONCLUSIONS

In this study, different types of ZnO morphologies including worm-like, nut-like and rod-like were synthesized by using the wet chemical method in the presence of cationic, anionic and nonionic surfactants, respectively. Structural analysis showed that all the samples had ZnO phase. Based on XRD result, the PEG-70 sample has some $Zn(OH)_2$ in addition to ZnO. FTIR spectra showed that the PEG-70 sample had stronger OH bond. Disc diffusion test and CFU method showed that the presence of surfactants in the synthesis of ZnO structures influenced the antibacterial activity of the samples. All the samples showed antibacterial activity. Moreover, PEG-70 sample showed the greatest inhibition against bacteria growth. Therefore, ZnO has a high potential to use as surface coating at various areas for applications such as inhibiting the attachment and growth of microorganisms and forming biofilms residing in medical devices.

5. ACKNOWLEDGMENTS

The authors are thankful to SARV Oil & Gas Industries Development Company for providing the necessary facilities to carry out this project. They also thank Dr. Keshavarz from SARV Oil & Gas Industries Development Company for his help in this project.

6. BIBLIOGRAPHY

[1] W. LIN, Z. XU, Z. WANG, J., *et al.*, "Influence of Bi3Zn2Sb3O14 pre-synthesis phase on electrical properties of the ZnO-Bi2O3 based varistor ceramics," *J. Alloys Compd.*, v. 834, p. 155070, 2020.

[2] SARANYA, A., DEVASENA, T., SIVARAM, H., *et al.* "Role of hexamine in ZnO morphologies at different growth temperature with potential application in dye sensitized solar cell," *Mater. Sci. Semicond. Process.*, v. 92, pp. 108-115, 2019.

[3] GAO, R., *et al.*, "Highly selective detection of saturated vapors of abused drugs by ZnO nanorod bundles gas sensor," *Appl. Surf. Sci.*, v. 485, pp. 266–273, 2019.

[4] CASAMASSA, E., FIORAVANTI, A., MAZZOCCHI, M., *et al.*, "Abrasive properties of ZnO: Influence of different nanoforms," *Tribol. Int.*, v. 142, p. 105984, 2020.

[5] SUBRAMANIAM, V.D., *et al.*, "Health hazards of nanoparticles: understanding the toxicity mechanism of nanosized ZnO in cosmetic products," *Drug Chem. Toxicol.*, v. 42, n. 1, pp. 84-93, 2019.

[6] KHERA, S., CHAND, P., "Influence of different solvents on the structural, optical, impedance and dielectric properties of ZnO nanoflakes," *Chinese J. Phys.*, v. 57, pp. 28-46, 2019.

[7] RAIZADA, P., SUDHAIK, A., SINGH, P. "Photocatalytic water decontamination using graphene and ZnO coupled photocatalysts: A review," *Mater. Sci. Energy Technol.*, v. 2, n. 3, pp. 509-525, 2019.

[8] RAHMANE, S., DJOUADI, M. A. "Optoelectronic properties of ZnO thin films grown by radio frequency magnetron sputtering," *J. Mater. Sci. Mater. Electron.*, v. 31, n. 20, pp. 17872-17878, 2020.

[9] SCHIFANO, E. *et al.*, "Antibacterial Effect of Zinc Oxide-Based Nanomaterials on Environmental Biodeteriogens Affecting Historical Buildings," *Nanomaterials*, v. 10, n. 2, 2020.

[10] YUSOF, N. A. A., ZAIN, N. M., PAUZI, N. "Synthesis of ZnO nanoparticles with chitosan as stabilizing agent and their antibacterial properties against Gram-positive and Gram-negative bacteria," *Int. J. Biol. Macromol.*, v. 124, pp. 1132-1136, 2019.

[11] SASANI GHAMSARI, M., ALAMDARI, S., HAN, W., *et al.* "Impact of nanostructured thin ZnO film in ultraviolet protection," *Int. J. Nanomedicine*, v. 12, p. 207, 2017.

[12] THEERTHAGIRI, J. *et al.*, "A review on {ZnO} nanostructured materials: energy, environmental and biological applications," v. 30, n. 39, p. 392001, Jul. 2019.

[13] TIWARY, P., MAHAPATRA, R., CHAKRABORTY, A. K. "ZnO nanobristles prepared by one-step thermal decomposition of zinc nitrate as ultra-high response ethanol sensor at room temperature," *J. Mater. Sci. Mater. Electron.*, v. 30, n. 6, pp. 5464-5469, 2019.

[14] LIANG, Q., QIAO, F., CUI, X., *et al.* "Controlling the morphology of ZnO structures via low temperature hydrothermal method and their optoelectronic application," *Mater. Sci. Semicond. Process.*, v. 89, pp. 154-160, 2019.

[15] VAHDAT VASEI, H., MASOUDPANAH, S. M., ADELI, M., *et al.*, "Mesoporous honeycomb-like ZnO as ultraviolet photocatalyst synthesized via solution combustion method," *Mater. Res. Bull.*, v. 117, pp. 72-77, 2019.

[16] ISMAIL, A. M., MENAZEA, A. A., KABARY, H. A., *et al.*, "The influence of calcination temperature on structural and antimicrobial characteristics of zinc oxide nanoparticles synthesized by Sol–Gel method," *J. Mol. Struct.*, v. 1196, pp. 332-337, 2019.

[17] IKHMAYIES, S. J. "Synthesis of Flower-Like ZnO Micro/Nano Structures by the Spray Pyrolysis Technique,"

JOM, v. 72, n. 2, pp. 621-627, 2020.
[18] NOMAN, M. T., PETRU, M., MILITKÝ, J., *et al.* "One-Pot Sonochemical Synthesis of ZnO Nanoparticles for Photocatalytic Applications, Modelling and Optimization," *Materials (Basel).*, v. 13, n. 1, 2020.
[19] GARINO, N. *et al.*, "A Microwave-Assisted Synthesis of Zinc Oxide Nanocrystals Finely Tuned for Biological Applications," *Nanomaterials*, v. 9, n. 2, 2019.
[20] EL-SHAARAWY, M. G., KHAIRY, M., MOUSA, M. A. "Structural, electrical and electrochemical properties of ZnO nanoparticles synthesized using dry and wet chemical methods," *Adv. Powder Technol.*, v. 31, n. 3, pp. 1333–1341, 2020.
[21] RAJAMANICKAM, S., MOHAMMAD, S. M., HASSAN, Z. "Effect of zinc acetate dihydrate concentration on morphology of ZnO seed layer and ZnO nanorods grown by hydrothermal method," *Colloid Interface Sci. Commun.*, v. 38, p. 100312, 2020.
[22] NIKAM, A. V., PRASAD, B. L. V., KULKARNI, A. A. "Wet chemical synthesis of metal oxide nanoparticles: a review," *CrystEngComm*, v. 20, n. 35, pp. 5091–5107, 2018.
[23] IQBAL, T. *et al.*, "Surfactant assisted synthesis of ZnO nanostructures using atmospheric pressure microplasma electrochemical process with antibacterial applications," *Mater. Sci. Eng. B*, v. 228, pp. 153-159, 2018.
[24] DEBANATH, M. K., KARMAKAR, S. "Study of blueshift of optical band gap in zinc oxide (ZnO) nanoparticles prepared by low-temperature wet chemical method," *Mater. Lett.*, v. 111, pp. 116-119, 2013.
[25] ZARE, M., NAMRATHA, K., BYRAPPA, K., *et al.* "Surfactant assisted solvothermal synthesis of ZnO nanoparticles and study of their antimicrobial and antioxidant properties," *J. Mater. Sci. Technol.*, v. 34, n. 6, pp. 1035-1043, 2018.
[26] SIRELKHATIM, A. *et al.*, "Review on Zinc Oxide Nanoparticles: Antibacterial Activity and Toxicity Mechanism," *Nano-Micro Lett.*, v. 7, n. 3, pp. 219–242, 2015.
[27] TALEBIAN, N., AMININEZHAD, S. M., DOUDI, M. "Controllable synthesis of ZnO nanoparticles and their morphology-dependent antibacterial and optical properties," *J. Photochem. Photobiol. B Biol.*, vol. 120, pp. 66–73, 2013.
[28] CHITRA, K. "Antimicrobial activity of wet chemically engineered spherical shaped ZnO nanoparticles on food borne pathogen," *Int. Food Res. J.*, v. 20, pp. 59-64, 2013.
[29] MA, J., LIU, J., BAO, Y., *et al.* "Synthesis of large-scale uniform mulberry-like ZnO particles with microwave hydrothermal method and its antibacterial property," *Ceram. Int.*, v. 39, pp. 2803-2810, 2013.
[30] RAMANI, M., PONNUSAMY, S., MUTHAMIZHCHELVAN, C., *et al.* "Morphology-directed synthesis of ZnO nanostructures and their antibacterial activity.," *Colloids Surf. B. Biointerfaces*, v. 105, pp. 24-30, May 2013.
[31] EL-NAHHAL, I. M., ELMANAMA, A. A., EL ASHGAR, N. M., *et al.* "Stabilization of nano-structured ZnO particles onto the surface of cotton fibers using different surfactants and their antimicrobial activity," *Ultrason. Sonochem.*, v. 38, pp. 478-487, 2017.
[32] LIU, B., ZENG, H. C. "Room Temperature Solution Synthesis of Monodispersed Single-Crystalline ZnO Nanorods and Derived Hierarchical Nanostructures," *Langmuir*, v. 20, n. 10, pp. 4196-4204, 2004.
[33] KAWANO, T., IMAI, H. "Fabrication of ZnO Nanoparticles with Various Aspect Ratios through Acidic and Basic Routes," *Cryst. Growth Des. - CRYST GROWTH DES*, v. 6, 2006.
[34] LIU, B., ZENG, H. C. "Hydrothermal synthesis of ZnO nanorods in the diameter regime of 50 nm.," *J. Am. Chem. Soc.*, v. 125, n. 15, pp. 4430–4431, Apr. 2003.
[35] SHABA, E. Y., JACOB, J. O., TIJANI, J. O., *et al.*. Suleiman, "A critical review of synthesis parameters affecting the properties of zinc oxide nanoparticle and its application in wastewater treatment," *Appl. Water Sci.*, v. 11, n. 2, p. 48, 2021.
[36] HASSAN BASRI, H., TALIB, R. A., SUKOR, R., *et al.* "Effect of Synthesis Temperature on the Size of ZnO Nanoparticles Derived from Pineapple Peel Extract and Antibacterial Activity of ZnO–Starch Nanocomposite Films," *Nanomaterials*, v. 10, n. 6, 2020.
[37] MOHAMMADI, F. M., GHASEMI, N. "Influence of temperature and concentration on biosynthesis and characterization of zinc oxide nanoparticles using cherry extract," *J. Nanostructure Chem.*, v. 8, n. 1, pp. 93–102, 2018.
[38] SUN, X. M., CHEN, X., DENG, Z. X., *et al.* "A CTAB-assisted hydrothermal orientation growth of ZnO nanorods," *Mater. Chem. Phys.*, v. 78, n. 1, pp. 99-104, 2003.
[39] RANA, S. B. "Influence of CTAB assisted capping on the structural and optical properties of ZnO nanoparticles," *J. Mater. Sci. Mater. Electron.*, v. 28, n. 18, pp. 13787-13796, 2017.
[40] LI, P., WEI, Y., LIU, H., *et al.*, "Growth of well-defined ZnO microparticles with additives from aqueous solution," *J. Solid State Chem.*, v. 178, n. 3, pp. 855-860, 2005.
[41] WANG, J., LIU, C., XIANG, L. "Influence of Sodium Dodecyl Sulfonate on the Formation of ZnO Nanorods from ε-$Zn(OH)_2$," *J. Nanomater.*, v. 2013, p. 621378, 2013.
[42] ZHANG, H., FENG, J., WANG, J. *et al.*, "Preparation of ZnO nanorods through wet chemical method," *Mater. Lett.*, v. 61, n. 30, pp. 5202-5205, 2007.
[43] SUDHA, M., SENTHILKUMAR, S., HARIHARAN, R., *et al.*, "Synthesis, characterization and study of

photocatalytic activity of surface modified ZnO nanoparticles by PEG capping," *J. Sol-Gel Sci. Technol.*, v. 65, n. 3, pp. 301-310, 2013.
[44] EADI, S. B., KIM, S., JEONG, S. W. "Effect of Surfactant on Growth of ZnO Nanodumbbells and Their Characterization," *J. Chem.*, v. 2017, p. 1728345, 2017.
[45] WAHAB, R., ANSARI, S. G., KIM, Y. S., *et al.*"Synthesis and characterization of hydrozincite and its conversion into zinc oxide nanoparticles," *J. Alloys Compd.*, v. 461, n. 1, pp. 66–71, 2008.
[46] THIRUGNANAM, T. "Effect of Polymers (PEG and PVP) on Sol-Gel Synthesis of Microsized Zinc Oxide," *J. Nanomater.*, vol. 2013, p. 362175, 2013.
[47] HSU, A. *et al.*, "Is the effect of surface modifying molecules on antibacterial activity universal for a given material?," *Nanoscale*, v. 6, n. 17, pp. 10323–10331, 2014.
[48] ESPITIA, P. J. P., SOARES, N. F. F., COIMBRA, J. S. R., *et al.* "Zinc Oxide Nanoparticles: Synthesis, Antimicrobial Activity and Food Packaging Applications," *Food Bioprocess Technol.*, v. 5, n. 5, pp. 1447–1464, 2012.
[49] NAIR, S. *et al.*, "Role of size scale of ZnO nanoparticles and microparticles on toxicity toward bacteria and osteoblast cancer cells," *J. Mater. Sci. Mater. Med.*, v. 20, n. 1, p. 235, 2008.

ORCID

Mobina Bazari https://orcid.org/0000-0002-0440-9124
Najmeh Najmoddin https://orcid.org/0000-0002-1085-665X